A High Torque Density Axial Flux SRM with Modular Stator

Y. Ebrahimi* and M. R. Feyzi*(C.A.)

Abstract: A novel structure of Switched Reluctance Motors (SRMs) is proposed. The proposed structure uses the benefits of the axial flux path, short flux path, segmental rotor, and flux reversal free stator motors all together to improve the torque density of the SRMs. The main geometrical, electrical and physical specifications are presented. In addition, some features of the proposed structure are compared with those of a state-of-the-art radial flux SRM, considered as a reference motor. Then, the proposed structure is modified by employing a higher number of rotor segments than the stator modules and at the same time, reshaped stator modules tips. Achieved results reveal that, compared with the reference motor, the proposed and the modified proposed motors deliver about the same torque with 36.5% and 46.7% lower active material mass, respectively. The efficiency and torque production capability for the extended current densities are also retained. These make the proposed structures a potentially proper candidate for the Electric Vehicles (EVs) and Hybrid Electric Vehicles (HEVs) as an in-wheel motor.

Keywords: Axial Flux Motors, Finite Element Method, In-Wheel Motors, Switched Reluctance Motors, Torque Density

1 Introduction

From flux path point of view, Switched Reluctance Motors (SRMs) are categorized into radial and axial flux path types. Comprehensive studies have been carried out on the radial flux motors. Some of these attempts are: giving variety to combination of number of stator and rotor poles; placing two saliencies per pole in the stator or the rotor; altering the stator or the rotor pole shape and size; introducing the stator with non-symmetrical poles; considering variant air gap length through the pole arc; introducing double stator motors and multi-layer motors. Making rotor segmented was one of the most important reformations of SRMs structure enabling them to deliver considerably high torque per volume ratio [1, 2]. Mecrow et al. introduced two different structures for radial flux segmental rotor SRMs and named them single-tooth winding segmental rotor SRM and multi-tooth winding segmental rotor SRM which can be abbreviated as STW and MTW, respectively. Whereas there are differences between the designs of these two types of machines, the fundamental operations are the same. It can be realized that the MTW needs longer end winding than STW. Since axial flux motors need longer end winding compared with radial flux motors, the length of the end winding is excessively large in case of the axial flux MTW. Therefore, STW is selected as the reference motor for design consideration and comparison purpose in the present study.

Despite the radial flux SRMs, less consideration has been shown to the axial flux ones. These structures are quite demanded for traction and propulsion applications as hub motors in which spatial constrains lead the motor dimensions to the large diameter and short stack length. For traction applications, SRMs present advantages in terms of cost compared to both rare earth permanent magnet brushless motors and induction machines [3]. In addition, they deliver high torque density [4].

A 12/8 single-stator, dual-rotor axial flux segmental rotor SRM with toroidal winding arrangement is introduced in [5], and more evaluations and optimizations were carried out in [6] by the same authors resulting 12/16 configuration. Reported in the later, a torque density equal to 1.83 Nm/kg has been achieved keeping the volume of the active materials equal to that of the STW in [1] with a different length to diameter ratio. This level of torque density has been reported high enough to make the case a proper candidate for the EV application.

It was recently shown that SRMs having a higher number of rotor poles than stator poles have higher efficiency and torque to mass ratio [7-9]. Different rotor/stator combinations effect on the motor torque and performance has been studied comprehensively in [8].

Iranian Journal of Electrical & Electronic Engineering 2015.
Paper first received 06 Mar. 2015 and in revised form 23 Aug. 2015.
* The Authors are with the Department of Electrical and Computer Engineering, Tabriz University, Tabriz, Iran.
Emails: y.ebrahimi@tabrizu.ac.ir and feyzi@tabrizu.ac.ir.

Reported results reveal that the optimized 12/14 one has the highest Nm/kg compared with the others.

In this paper, a novel three-phase, 12/10, segmental rotor, modular stator, and axial flux SRM is presented. The Finite Element Method (FEM) is used to analysis the proposed motor. Whereas the static analyses are carried out by both 3D and quasi-3D models, the transient analyses are carried out only by quasi-3D model. Accuracy of quasi-3D modeling is evaluated by both 3D modeling and experimental results of the mentioned reference motor (i.e. STW) from [1] in which all the geometric parameters, the electrical specifications and the material properties are well documented. As a next step, the proposed structure is modified by using a higher number of rotor segments than the stator modules (12/14) and modified shape of the narrow modules tip of the stator. This modification improves the flux path for different rotor positions by avoiding the local highly deep saturation in the stator narrow module tip. Additionally, this configuration results in considerable reduction of core iron mass, especially in the stator in which the major part of the iron loss appears. There is no degradation in the motor output torque as the major considered performance criterion of the motor in this work. These result in a high torque per active material mass (Nm/kg) SRM.

2 Proposed Motor

2.1 Geometric Details

Seeking an electromechanical system with the shortest flux path and the high degree of available space utilization leads to that shown in Fig. 1. The upper and lower parts can be considered as two translating parts of the system supposing the winding and the vertical arms of the core as the stationary parts. Quasi-3D model of axial flux switched reluctance motor is resulted in by repeating each of the translating and stationary parts in a proper number. Cyclic 3D view of this motor can be seen in Fig. 2 where the 1/4 of the stator and rotor are shown. This is considered as the proposed axial flux segmental switched reluctance motor in this paper. The flux paths are shown in this figure at the both aligned and unaligned positions of the rotor. As mentioned, the flux path is as short as possible, and the stator can be flux reversal free resulting in low core losses. Geometric parameters of the motor are listed in Table 1 (refer to Fig.1). Presented formulas can be easily extracted from this figure. The parameter C is defined as the slot opening factor, and determines the rotor pole arc to rotor pole pitch ratio. Both of the stator and rotor are segmented, and no back iron is required for closing the flux path or providing a mechanical support. In fact, the stator modules are mounted on the shaft utilizing a special interface assembly. The connection regions for the stator modules are two surfaces of the module tips at the inner radius of the laminations. Rotor segments are inlayed in a solid disc with a nonmagnetic material (e.g. S316).

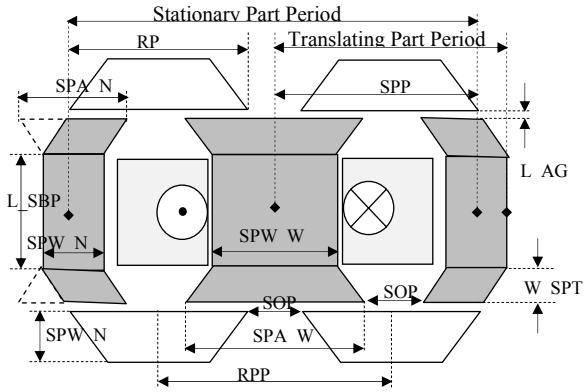

Fig. 1 Representation of geometric parameters.

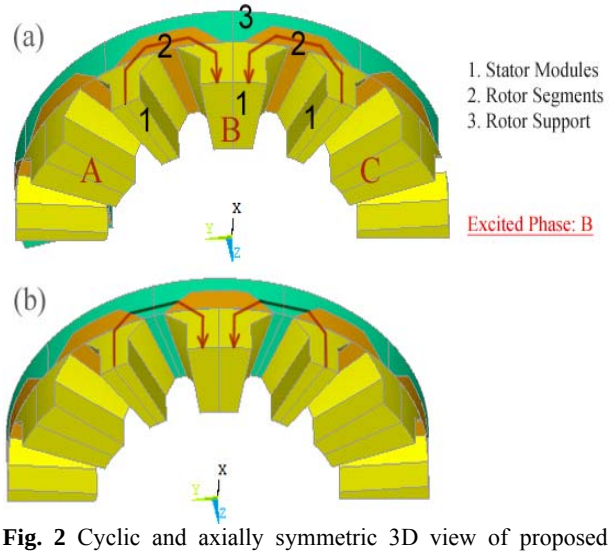

Fig. 2 Cyclic and axially symmetric 3D view of proposed axial flux segmental SRM, (a) Rotor aligned position (b) Rotor unaligned position.

Two rotors are connected to each other to form a totally enclosed enclosure encompassing the stator. The stator is firmed on a hollow stationary shaft so that the necessary winding terminals can be taken out through it. The valid combinations of the stator module/rotor segment numbers can be expressed as

$$N_{seg,sttr} = N_{ph} x N_c$$
$$N_{seg,rtr} = (N_{ph} x \pm 1) N_c \quad (1)$$

where N_{ph}, N_c, x, $N_{seg,sttr}$, and $N_{seg,rtr}$ are the number of phases, the number of coils per phase, a positive even integer, the number of stator segments, and the number of rotor segments, respectively. Some feasible combinations are 12/10, 12/14, 18/15, and 18/21. In this paper, 12/10 one is selected for comparison with the reference STW motor. Deciding on the proper combination strongly depends on the application in which the machine is employed.

Table 1 Geometric parameters of the motor (Fig. 1).

Parameter	Symbol	Value
Stator Pole Pitch	SPP	360/Ns
Rotor Pole Pitch	RPP	360/Nr
Rotor Pole Arc	RPA	C*RPP
Stator Wide Pole Arc	SPA_W	C*RPP
Stator Narrow Pole Arc	SPA_N	2*(SPP-RPP)+ SPA_W
Slot Opening	SOP	RPP*(1-C)
Stator Wide Pole Width	SPW_W	from design
Stator Narrow Pole Width	SPW_N	from design
Length of Air-gap	L_AG	from design
Width of Stator Pole Tip	W_SPT	from design
Length of Stator Pole Base Part	L_SBP	from design

2.2 Output Torque Equation

Output torque derivation procedure of axial flux SRMs has been presented in [5] and [6]. Similar procedure can be customized and employed for proposed motor. The average torque developed by the non-saturated motor is expressed as

$$T_{avg} = \frac{1}{2} I_{ph}^2 \frac{\Delta L}{\varepsilon} = \frac{1}{2} I_{ph}^2 \frac{(L_a - L_u)}{\varepsilon} \quad (2)$$

where L_a is the phase self-inductance at aligned position, L_u is the phase self-inductance at unaligned position, and ε is the stroke angle. The torque equation is

$$T_{avg} = \frac{1}{2\varepsilon} I_{ph}^2 L_a k \quad (3)$$

by defining k as $1\text{-}L_u/L_a$. For proposed motor L_a is

$$L_a = \frac{4 B_g A_{ovl} N_{ph}}{I_{ph}} \quad (4)$$

where N_{ph} is the number of winding turn per phase, B_g is the average air-gap flux density at the aligned position, and A_{ovl} is the overlap area between the stator and rotor segments that is expressed as

$$L_a = \frac{4 B_g A_{ovl} N_{ph}}{I_{ph}} \quad (5)$$

where D_o and D_i are outer and inner diameters of the core steel, respectively. Substituting Eqs. (4) and (5) in Eq. (3) gives

$$T_{avg} = \frac{1}{4} I_{ph} N_{ph} B_g k (D_o^2 - D_i^2) \quad (6)$$

Defining $D_{avg}=(D_o+D_i)/2$ as the average diameter of the core laminations and $L_{act}=(D_o-D_i)$ as the active length of the core laminations, the average torque of the proposed motor is

$$T_{avg} = \frac{1}{2} I_{ph} N_{ph} B_g k D_{avg} L_{act} \quad (7)$$

where l_g is the air-gap length. Finally the average air-gap flux $_{density}$ at the aligned position is

$$B_g = \frac{N_{ph} I_{ph} \mu_0}{8 l_g} \quad (8)$$

3 Modified Proposed Motor

As mentioned in section 1, the higher number of rotor segments than the stator poles (or modules in the proposed motor) can improve the motor torque production capability. Here the 12/14 combination is selected as a consequence of the study accomplished in [8]. For proposed motor, the stator wide and narrow poles arcs are selected similar to those of STW motor. It makes the comparison of two motors performance dependent only on two motors topology by removing the influence of these two geometric parameters. These parameters are dependent on the slot opening factor, C. So, it is essential to understand the effect of C on the output torque, considered as the major performance criterion of the motor in this paper. The expression of instantaneous torque production of an SRM phase can be written as

$$T_{inst} = N_{ph} I_{pk} \frac{\partial \varphi}{\partial \theta} - \frac{\partial W_f}{\partial \theta} \quad (9)$$

where W_f is stored field energy. The influence of the second term of Eq. (9) is small due to deep saturation in SRMs, and can be ignored. So, the average torque of the motor during one stroke is

$$T_{avg} = \frac{1}{\varepsilon} N_{ph} I_{pk} \varphi_a \left(1 - \frac{\varphi_u}{\varphi_a}\right) \quad (10)$$

here φ_a and φ_u are the aligned and unaligned phase flux, respectively. φ_a can be written as

$$\varphi_a = B_g A_{ovl} \quad (11)$$

where A_{ovl} is the overlap area of the rotor segment and stator module at aligned position which can be given in terms of geometric parameters as

$$A_{ovl} = \left(\frac{D_o - D_i}{2}\right)\left(\frac{D_o + D_i}{4}\right)\left(\frac{RPA - SOP}{2}\right) \quad (12)$$

Replacing C=RPA/SOP in Eq. (12) results in

$$A_{ovl} = \left(\frac{D_o^2 - D_i^2}{16}\right)(2C - 1)RPP \quad (13)$$

Replacing Eqs. (11) and (12) in Eq. (10) results in average torque as

$$T_{avg} = N_{ph} I_{pk} B_g \left(\frac{D_o^2 - D_i^2}{16}\right)(2C - 1)\left(1 - \frac{\varphi_u}{\varphi_a}\right) \quad (14)$$

This equation reveals that the motor average torque is increased with an increment in slot opening factor, C ($0.5<C<1$). It should be noted that φ_u is a nonlinear function of C too. Therefore, it is needed to employ FEA method to assess the torque variation as a function

of the slot opening as carried out in [9]. It is quite reasonable to suppose an identical slot opening factor for all under comparison motors to eliminate its influence on the comparison results. The slot opening factor is about 0.847 for the reference STW (12/10) motor. Substituting C = 0.847 for modified 12/14 motor in the formulas represented in Table 1 results in SPA_W=21.8 and SPA_N=30.4, both in mechanical degrees. It can be seen that the narrow modules of the stator have wider arc which imposes very sharp pole tip angles, wherein the tightened flux path results in a higher reluctance for various rotor positions. Consequently, less torque can be achieved for a given phase mmf. Therefore, it is required to modify the narrow pole tip shape in order to provide a flux path with unvarying width to avoid very deep localized saturation.

In this regard, the pole tip height should be equal to the stator narrow pole width (SPW_N) of the first layer of the computation planes, laid on the inner radius of the motor. This is equal to the rotor segments thickness.

Table 2 Geometric parameters, electrical specifications and material properties of three compared motors.

Parameter	STW Motor	Proposed Motor	Modified Proposed Motor
No. of Stator Poles/Modules	12	12	12
No. of Rotor Segments	10	10	14
No. of Phases	3	3	3
Lamination Outer Diameter, D_o(mm)	150	216.2	216.2
Active Material Axial Length, L (mm)	150	63.8	53.8
Air-gap Length (mm)	0.3	0.3	0.3
Bore/Average Air-gap Diameter (mm)	90.8	170.6	170.6
Stator Wide Module Arc Pitch (deg.)	30.5	30.5	21.8
Stator Narrow Module Arc Pitch (deg.)	18.5	18.5	30.4
Rotor Segment Pitch (deg.)	30.5	30.5	21.8
No. of Turns per Phase	270	548	548
Phase Resistance, @20^{0}C (Ω)	2.56	2.57	2.57
Slot Fill Factor (%)	41	41	41
Estimated Turn Length (mm)	435	214	214
End Winding Length per Turn (mm)	135	123	123
Effective Wire Diameter (mm)	1	1	1
Motor $D_o^2 * L$ (mm^3)	3.375e06	2.986e06	2.515e06
Core Material	M270-35	M270-35	M270-35

The stator modules width and axial length of the motor are selected in a way that the space for coils is kept unchanged for all three motors, and the flux density of various parts of the core has a reasonable value. Then the number of the phase coil turns is designed such that almost identical phase resistance is achieved for three motors. Indeed, comparison is based on the identical copper loss for all motors. Table 2 gives geometric and electrical details of three motors. The linearized 2D model of modified geometry will be shown in the simulation results of the modified proposed motor. It should be noted that the proposed and modified proposed motors are preliminarily evaluated in this paper, and are not optimized.

4 Simulation Results

From the point of quasi-3D modeling view, the axial flux SRM can be considered to be composed of several linear machines. The overall performance of the machine is obtained by summing the performance of individual linear machines located on computation planes [10]. Based on the procedure introduced in [10], quasi-3D model of the proposed motor is prepared in five computation planes and simulated by using of the same method applied to the reference motor. Fig. 3 shows the static torque of the middle layer alongside the average of the all layers. Results reveal that the static torque of the middle layer of the quasi-3D model is in an intensive agreement with the average ones of all layers.

Fig. 4 shows the magnetic flux distribution for the middle layer of quasi-3D model of proposed motor. In the proposed motor, coils width is constrained by the stator wide and narrow modules at the inner radius of the motor. So, there is some distance between the coils and the stator narrow modules in Fig. 4 in which the middle layer of the model is represented.

Convergence of the results achieved from two different magnetic field formulations is introduced as a simulation accuracy test technique in some FEA tools (e.g. ANSYS software).

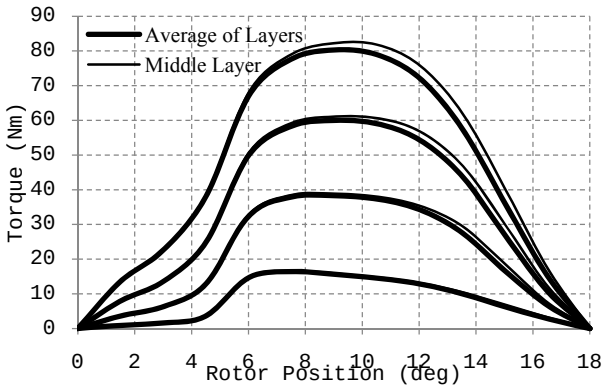

Fig. 3 Static phase torque curves for proposed motor obtained from quasi-3D FEM modeling (Each curve is for a constant current, rising in 5.0 A steps to 20.0 A).

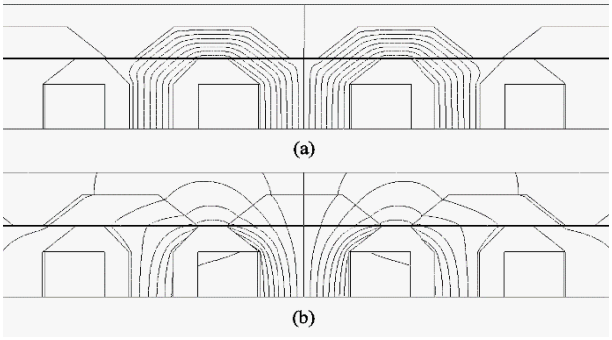

Fig. 4 Magnetic flux distribution of proposed motor (Quasi-3D, VMP method) (a) Rotor aligned position (b) Rotor unaligned position.

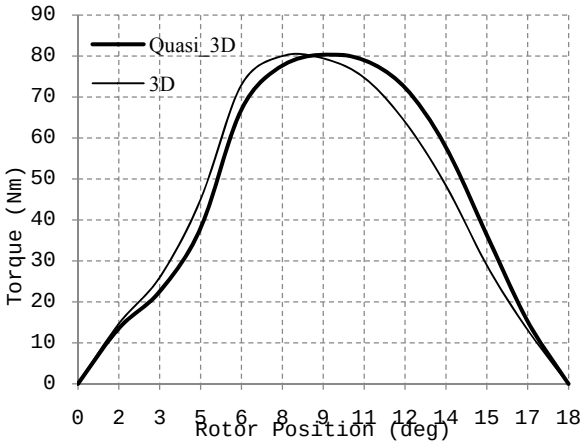

Fig. 5 Static torque curves for proposed motor i=20.0A (comparison of 3D and quasi-3D FEM modeling)

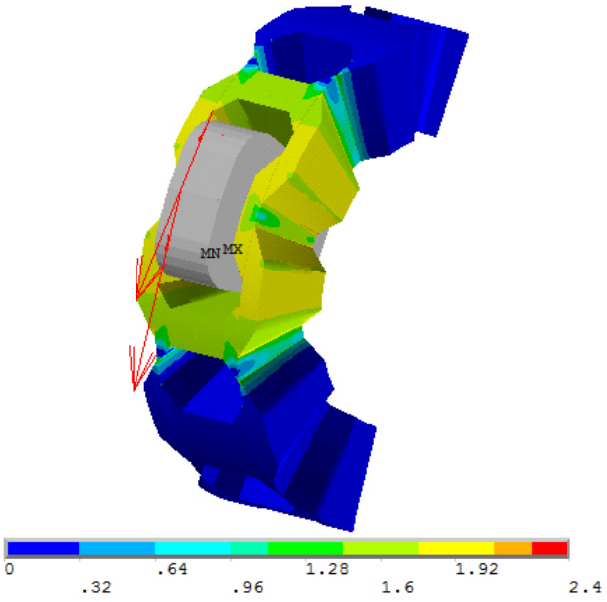

Fig. 6 Cyclic shaded plot of magnetic flux density for proposed motor (SMP method).

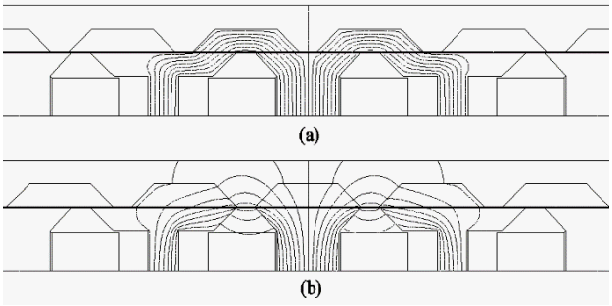

Fig. 7 Magnetic flux distribution of modified proposed motor (Quasi-3D, VMP method), (a) Rotor aligned position (b) Rotor unaligned position.

So, as an alternative measure, a 3D model of the proposed motor is prepared and simulated by using of scalar magnetic potential (SMP) formulation.

Fig. 5 shows that the obtained results from quasi-3D and 3D models by using two different formulations are in an acceptable agreement. 3D view of the shaded plot of the magnetic flux density at the rotor aligned position is shown in Fig. 6. In this figure, only the active material parts of the motor are shown.

Quasi-3D model of the modified proposed motor was constructed based on the details explained in part 3. Figure 7 shows the magnetic flux distribution for the middle layer of quasi-3D model of modified proposed motor for both aligned and unaligned positions. This figure shows the modified narrow pole tip in which a path with unvarying width is provided for magnetic flux. Static characteristics of the motor are shown in Fig. 8. It can be seen that the modified proposed motor is able to deliver almost the same torque for an identical exiting phase current. Fig. 9 shows flux linkage/phase current loci for STW and two proposed motors, operating at low speed under current control with a phase current level related to 300 W of copper loss (9.53 A at 100 ºC of average winding temperature).

Each phase is carrying constant current of 9.53 A for one third of the electrical cycle. Switches on/off angles are selected in a way that the maximum average torque can be achieved.

It corresponds to switch on 40 electrical degrees after the unaligned position, and switch off 20 degrees before the aligned position for both STW and Proposed motors, and switch on 30 electrical degrees after the unaligned position, and switch off 30 degrees before the aligned position for the modified proposed motor. The area of these loci is related to torque production of the motor per each stroke. It should be noted that whereas the modified proposed motor experiences 14 strokes during each rotor revolution, this is equal to 10 for the other two motors, so that this machine produces 40% more torque per unit area of the locus.

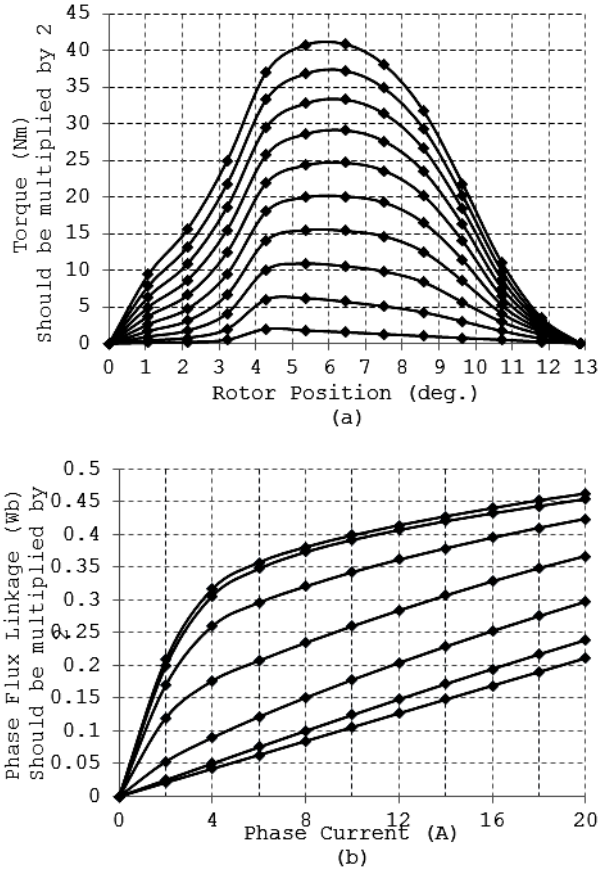

Fig. 8 Static characteristics of modified proposed motor (Quasi-3D FEM modeling), (a) Static phase torque (Each curve is for a constant current, rising in 2.0 A steps to 20.0 A) (b) Static phase flux linkage (Each curve is at constant position, from unaligned to aligned positions in 3.0 deg. Steps).

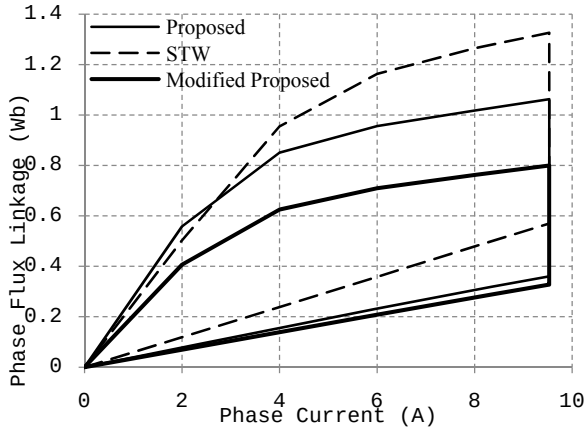

Fig. 9 Flux-linkage loci for three motors, operating under current control with a winding loss of 300 W (phase current = 9.53 A).

Table 3 gives the active material mass and the mean torque produced at 300 W of winding loss for two proposed motors alongside those for the STW motor.

Table 3 Mass and Nm/Kg comparison of motors.

	STW	**Proposed**	**Modified proposed**
Stator Iron Mass (kg)	9.23	4.37	3.43
Rotor Iron Mass (kg)	2.46	2.26	1.79
Total Iron Mass (kg)	11.69	6.63	5.22
Copper Mass (kg)	2.16	2.16	2.16
Total Active Mass (kg)	13.85	8.79	7.38
Avg. Torque (Nm), @300W of Copper Loss	26.5	26.3	26.2
Torque per Unit Active Mass (Nm/kg)	1.91	2.99	3.55

Whilst the proposed and the modified proposed motors deliver almost the same torque as the STW motor, they use 36.5% and 46.7% less active materials, respectively. In other words, since the copper mass is kept to be identical for all motors, these values can be translated as; STW motor employs 76% and 124% more core lamination than the proposed and the modified proposed motors, respectively to be able to deliver the same output torque. In order to obtain mean torques, the average winding temperature of 100 ºC is supposed. Also, it is assumed that the motor operates under current control scheme with one phase conducting at a time. Throughout the phase conduction period the phase is assumed to conduct a constant current and the torque output is based on the mean torque over the period of conduction.

In order to get more extensive sight, the mean torque per unit active material mass (Nm/kg) of some studied motors in various reference literatures is shown graphically in Fig. 10.

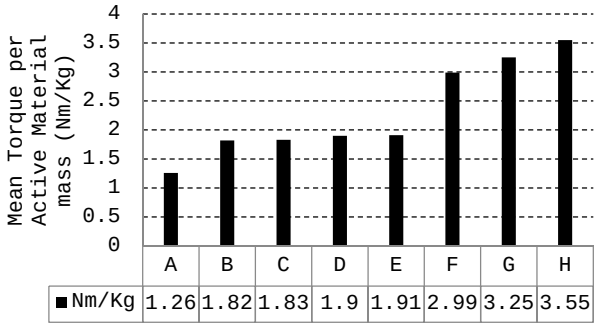

Fig. 10 Mean torque per active material mass (Nm/kg) of some studied motors in literatures;
A: Conventional (12/8), [8]
B: AFSSRM (12/8), [5]
C: AFSSRM (12/16), [6]
D: STW (12/10, Experimental), [1]
E: STW (12/10, Modeled in This Paper)
F: Proposed (12/10)
G: STW (12/26, Outer Rotor), [9]
H: Modified Proposed (12/14)

The proposed motors have a considerable high torque per active mass ratio compared with the others. The only exception is the proposed motor in [9]. This is a 12/26, radial flux, segmented, and outer rotor SRM with the single tooth windings. It should be emphasized once more that the proposed and the modified proposed motors are preliminarily evaluated in this paper, and have not been optimized.

The static analysis is performed for all layers of the quasi-3D model to obtain the overall static torque and phase flux linkage of the motor. The same procedure is not applicable to the transient analysis. Results derived from the static analysis reveal that the torque and the flux linkage characteristics of the middle layer of the quasi-3D model are in an intensive accordance with the average ones of the all layers, as can be seen in Fig. 3. Consequently, as long as the motor geometry is extruded radially (i.e. neither segments nor modules are parallel-sided), the middle layer can be considered as the representative layer of the motor for transient analysis.

The transient performance of the proposed motor is evaluated by coupling the quasi-3D FEM model of the motor with MATLAB/Simulink. The conventional asymmetric half-bridge converter is used to supply currents to the motor. Additional resistance and inductance are added in series to each phase coil to take the end windings effects into account. These two can be derived from static analysis alongside with data extracted from 3D model. An operating point should be selected to evaluation of the performance of the motors. The operating point depicted in [1] is selected as a reference where the control parameters are adjusted such that the copper loss and shaft torque are approximately 300 W and 30 Nm, respectively. Hysteresis current controller is used to regulate the phase currents. Hysteresis band width is ±0.2 for the reference current maintained at 10 A. Operational conditions in terms of motor speed, turn-on and turn-off angles are fixed for all motors as those of the STW in [1]. Table 4 gives the simulated performance parameters of the motor. Whereas the proposed and the modified proposed motors use 36.5% and 46.7% less active material mass, they have almost identical performance from torque production and efficiency points of view. It should be noted that the selected operating point is not necessarily the point in which the motors operate at their maximum efficiencies.

As represented in Table 2, the slot fill factor of both proposed motors were pessimistically assumed to be 41%. In fact, due to the modular structure of the stator and the rectangular cross section of slots, the slot fill factor of 75% is not unreasonable [11]. In case of the constant number of the phase coil turns, this assumption may result in about 45% reduction in the copper loss and consequently 5.7% of increment in the efficiency of the modified proposed motor.

Table 4 Performance comparison of motors.

	STW	**Proposed**	**Modified Proposed**
Speed (rpm)	586	586	586
Torque (Nm)	28.9	28.3	29.1
Stator Iron Loss (W)	69	29.5	42.1
Rotor Iron Loss (W)	14.5	20.3	17.9
Total Iron Loss (W)	73.5	49.8	60
Copper Loss (W)	307	315	307
Total loss (W)	380.5	365	367
Efficiency (%)	82.3	82.6	82.9

4.1 Comparison of Overload Capacity

An increase in the stator current results in enhanced mechanical power delivered to the shaft. This enhancement depends on the operating point of the motor. The incremental converted mechanical energy per stroke to the incremental input current ratio, G_{mi}, can be written as

$$G_{mi} = \frac{\Delta W_m}{\Delta i} = \lambda_0 + i_{s0}(L_s - L_u) + \frac{\Delta i}{2}(L_s - L_u) \qquad (15)$$

where λ_0 is the intercept on the flux linkages axis from the saturated portion of the aligned position curve, L_u is unaligned inductance per phase, L_s is the incremental aligned inductance per phase, i_{so} is the operating stator current at which the incremental values are calculated, Δi denotes the incremental stator current, and ΔW_m is the resulting mechanical energy per stroke [12]. In SRMs, $L_u \geq L_s$; larger L_u/L_s means higher rate of diminishing in torque production capability with increasing phase exciting current. In other words, G_{mi} decreases as the saturation level increases. This means that, in the highly saturated regions, the energy conversion capability of the motor is reduced. As a result, a maximum exciting current should be selected in order to preserve desired performance of the motor. Accordingly, an appropriate cooling system should be designed. Fig. 11 shows Flux linkages versus stator current of STW and both proposed motors.

Exciting current level is extended up to 20 A which corresponds to 1320 W of copper loss and 8.5 A/mm^2 of current density in these under comparison motors by assuming an appropriate cooling system. It can be seen that L_u/L_s in the proposed motor is smaller than STW. As a result, the proposed motor can deliver more torque at the high levels of exciting current, as shown in Fig. 12. This figure shows that the proposed motor is able to deliver 5.5% more torque at 20 A (8.5 A/mm^2) of exciting current level. For a liquid-cooled machine, 20 A/mm^2 of current density is completely reasonable. So, increment of current density up to this level leads to the more diminishing in torque production rate of STW motor.

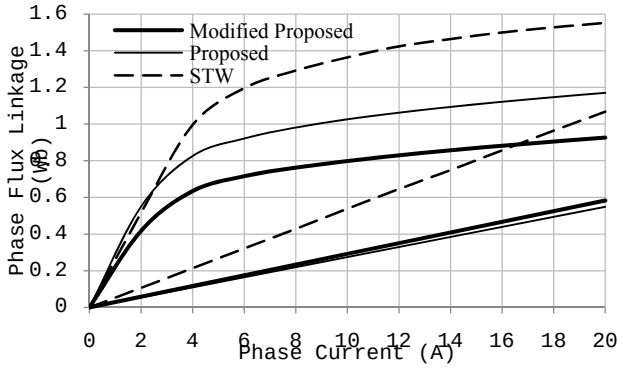

Fig. 11 Phase flux linkages versus stator phase current

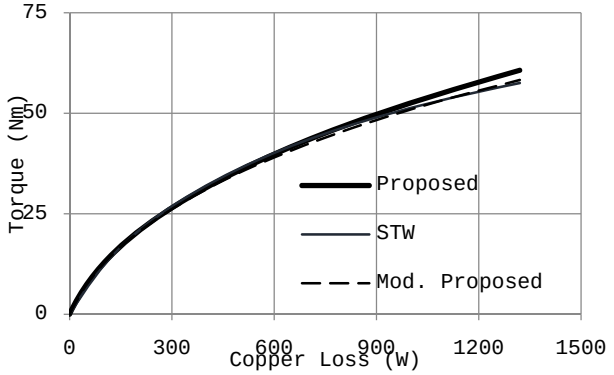

Fig. 12 Variation of torque with copper loss.

Consequently the proposed motor can be considered as a more appropriate candidate for low voltage and high current applications. Lower overload capacity is considered as a potential drawback of segmental SRMs especially with the higher number of rotor segments [9]. An increment in the number of rotor segments for a given number of stator slots leads to the higher degree of rotor segments proximity. The closeness of segments causes the higher L_u/L_s ratio, especially for higher current densities, since the increased leakage flux between the rotor segments results in the higher inductance at unaligned position. Consequently, a reduction in overload capacity is expected for 12/14 modified proposed motor in comparison with 12/10 proposed motor as can be seen in Fig. 12. This figure shows that the modified proposed motor has almost identical overload capacity compared with STW motor even with the higher number of rotor segments.

5 Conclusion

A high torque density axial flux segmental SRM with modular stator was presented in details. Simulation results of a radial flux segmented SRM with Single Tooth Winding (STW) were compared with the experimental results as a measure to confirm the accuracy of the simulation method applied in the present paper. As another measure, 3D and quasi-3D simulation results of the proposed motor were compared. Then the proposed motor was modified by increasing the number of rotor a segments and reshaping the stator narrow module tips.

It is found that, whereas the proposed and the modified proposed motors use 36.5% and 46.7% less active materials mass, they show almost identical performance from torque production and efficiency points of view. The modified proposed motor exhibits a very high torque per active material mass ratio (3.55 Nm/kg). The Proposed motor has higher overload capacity than STW, and there is no degradation in overload capacity of the modified proposed motor in spite of the higher number of rotor segments in comparison with STW. These make both of proposed motors potentially proper candidates for electric vehicles (EVs) and the hybrid electric vehicles (HEVs) as in-wheel motors. A prototype of modified proposed motor is under construction and a comprehensive study including thermal analysis will be reported in the future work.

References

[1] B. C. Mecrow, E. A. El-Kharashi, J. W. Finch and A. G. Jack, "Segmental rotor switched reluctance motors with single-tooth windings", *IEE Proc-B*, Vol. 150, No. 5, pp. 591–599, 2003.

[2] B. C. Mecrow, E. A. El-Kharashi, J. W. Finch and A. G. Jack, "Preliminary Performance Evaluation of Switched Reluctance Motors with Segmental Rotors", *IEEE Transactions on Energy Conversion,* Vol. 19, No. 4, pp. 679–686, 2004.

[3] D. G. Dorrell, "Comparison of different motor design drives for hybrid electric vehicles", in *Energy Conversion Congress and Exposition (ECCE),* pp. 3352-3359, 12-16 September, Georgia, 2010.

[4] H. Neudorfer, "Comparison of three different electric powertrains for the use in hybrid electric vehicles", *4th IET Conference. on Power Electronics, Machines and Drives,* pp. 510-514, 2008.

[5] R. Madhavan and B. G. Fernandes, "A novel axial flux segmented SRM for electric vehicle application", *in proc. International Conference on Electrical Machines*, pp. 1–6, Rome, Italy, 6-8 September 2010.

[6] R. Madhavan and B. G. Fernandes, "Axial Flux Segmented SRM with a Higher Number of Rotor Segments for Electric Vehicles", *IEEE Transactions on Energy Conversion*, Vol. 28, No. 1, pp. 203–213, March. 2013.

[7] P. C. Desai, M. Krishnamurthy, N. Schofield and A. Emadi, "Novel switched reluctance machine configuration with higher number of rotor poles than stator poles: Concept to implementation", *IEEE Transactions on Industrial Electronics*, Vol. 57, No. 2, pp. 649–659, Feb. 2010.

[8] J. D. Widmer and B. C. Mecrow, "Optimized Segmental Rotor Switched Reluctance Machines with a Greater Number of Rotor Segments than Stator poles*", IEEE Transactions on Industrial Application,* Vol. 49, No. 4, pp. 1491-1498, Jul. /Aug. 2013.

[9] V. Rallabandi and B. G. Fernandes, "Design Procedure of Segmented Rotor Switched Reluctance Motor for Direct Drive Applications", *IET Electric Power Application*, Vol. 8, No. 3, pp. 77–88, 2014.

[10] A. Parviainen, M. Niemela and J. Pyrhonen, "Modeling of axial flux permanent-magnet machines", *IEEE Transactions on Industrial Application*, Vol. 40, No. 5, pp. 333–1340, Sep/Oct. 2004.

[11] M. F. Momen and I. Husain, "Design and Performance Analysis of a Switched Reluctance Motor for Low Duty Cycle Operation", *IEEE Transactions on Industrial Application*, Vol. 41, No. 6, pp. 1612–1618, Nov./Dec. 2005.

[12] R. Krishnan, R. Arumugam and J. F. Lindsay, "Design Procedure for Switched-Reluctance Motors", *IEEE Transactions on Industrial Application*, Vol. 24, No. 3, pp. 456–461, May/June 1988.

Yousef Ebrahimi received his B.Sc. in control engineering from Sahand University of Technology, Tabriz, Iran, in 2001, and the M.Sc. in electrical engineering from Tabriz University, Tabriz, Iran, in 2008. He is pursuing his Ph.D. on electrical machine design since 2010 in the same university. His research interests are magnetic and thermal design and analysis of special electric machines with focus on SRMs. He is also interested in finite element analysis.

Mohammad Reza Feyzi received his B.Sc. and M.Sc. in 1975 from university of Tabriz in Iran with honor degree. He worked in the same university during 1975 to 1993. He started his Ph.D. work in the University of Adelaide, Australia in 1993. Soon after his graduation, he rejoined to the University of Tabriz. Currently, he is a professor in the same university. His research interests are finite element analysis, design and simulation of electrical machines and transformers.